Is Low-Temperature Creep of Asphalt Mastic Independent of Filler Shape and Mineralogy?—Arguments from Multiscale Analysis

Roman Lackner[1]; Markus Spiegl[2]; Ronald Blab[3]; and Josef Eberhardsteiner[4]

Abstract: This paper focuses on the effect of filler on the low-temperature creep of asphalt mastic. Based on experimental results obtained from bending-beam rheometer (BBR) experiments for both pure bitumen and mastic characterized by different filler types and content, a recently proposed multiscale model is employed for the prediction of low-temperature creep properties of the bitumen-filler composite. Accounting for the distinct matrix-inclusion morphology present at the so-called *mastic*-scale, the Mori–Tanaka scheme is employed for homogenization. This homogenization scheme is applied to the bitumen-filler composite, giving insight into the effect of filler on the low-temperature behavior of mastic. Hereby, the filler particles are considered as rigid inclusions with spherical shape, resulting in excellent agreement between the creep parameters of the homogenized material and the respective experimental BBR results. This agreement indicates that only the volume fraction of the filler, entering the Mori–Tanaka scheme, and neither the filler geometry nor the chemical composition of the filler influence low-temperature creep of asphalt mastic.

DOI: 10.1061/(ASCE)0899-1561(2005)17:5(485)

CE Database subject headings: Bitumen; Asphalts; Fills; Creep; Temperature.

Introduction

Low-temperature creep of asphalt provides the stress relaxation capacity in flexible pavements required to avoid cracking as a consequence of thermal shrinkage during cold winter periods. The viscosity of asphalt and, hence, its creep capacity, are mainly linked to the rheological behavior of the employed binder material, the bitumen. In order to describe the mechanical behavior of different types of bitumen and various asphalt mixtures, a multiscale model for asphalt—comprised of five scales of observation (see Fig. 1)—is employed. Hereby, at the lowest (*bitumen*-) scale, with a characteristic length of a few μm, the material is composed of clusters of large-scale molecules (asphaltenes) distributed in the maltene matrix (Shell-Bitumen-U.K. 1990; Jäger 2004). At the next higher scale, the so-called *mastic*-scale, the filler, i.e., aggregates with a diameter lower than 125 μm, is introduced. At the *mortar*-scale (see Fig. 1), the mastic is considered as a material phase with on-average constant material properties. The input data for multiscale models, such as the one shown in Fig. 1, are the mechanical properties, the volume fractions, and the shape of and the interaction between different constituents (asphaltenes, maltenes, filler, etc.). By means of upscaling information from one to the next higher scale of observation, it is aimed to finally obtain macroscopic material parameters for macroscopic analyses of flexible pavements.

In this paper, an upscaling procedure for parameters describing low-temperature creep of the bitumen-filler composite at the *mastic*-scale is presented. The experimental basis is provided by bending-beam experiments, conducted for different types of bitumen and filler. In the following section, the considered types of bitumen and filler are briefly described and basic information regarding the employed experimental setup is provided. Thereafter,

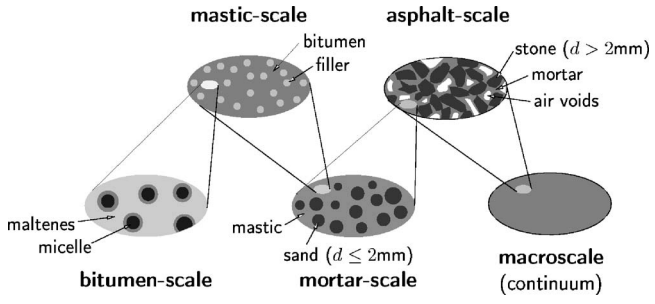

Fig. 1. Multiscale model for asphalt comprising five scales of observation

[1]University Dozent, Christian Doppler Laboratory for "Performance-Based Optimization of Flexible Pavements," Institute for Mechanics of Materials and Structures, Vienna Univ. of Technology, Karlsplatz 13/202, A-1040 Vienna, Austria. E-mail: roman.lackner@tuwien.ac.at

[2]Research Assistant, Christian Doppler Laboratory for "Performance-Based Optimization of Flexible Pavements," Institute for Road Construction and Maintenance, Vienna Univ. of Technology, Gußhausstraße 28/233, A-1040 Vienna, Austria. E-mail: mspiegl@istu.tuwien.ac.at

[3]Associate Professor, Christian Doppler Laboratory for "Performance-Based Optimization of Flexible Pavements," Institute for Road Construction and Maintenance, Vienna Univ. of Technology, Gußhausstraße 28/233, A-1040 Vienna, Austria. E-mail: rblab@istu.tuwien.ac.at

[4]Professor, Christian Doppler Laboratory for "Performance-Based Optimization of Flexible Pavements," Institute for Mechanics of Materials and Structures, Vienna Univ. of Technology, Karlsplatz 13/202, A-1040 Vienna, Austria. E-mail: josef.eberhardsteiner@tuwien.ac.at

Note. Associate Editor: Mary Stroup-Gardiner. Discussion open until March 1, 2006. Separate discussions must be submitted for individual papers. To extend the closing date by one month, a written request must be filed with the ASCE Managing Editor. The manuscript for this paper was submitted for review and possible publication on August 10, 2004; approved on October 29, 2004. This paper is part of the ***Journal of Materials in Civil Engineering***, Vol. 17, No. 5, October 1, 2005. ©ASCE, ISSN 0899-1561/2005/5-485–491/$25.00.

Table 1. Characteristics of Bitumens Considered in the Experimental Program (SBS: Styrene-Butadiene-Styrene)

Type of bitumen	Characterization	Penetration depth [1/10 mm]	Breaking point [°C]	Softening point [°C]
B90/10	Hard (air-blown) bitumen	7	4	87
B50/70	Standard bitumen	49	−13	51
B70/100	Standard bitumen	72	−17	47
B160/220	Soft bitumen	151	−17	40
pmB60/90	SBS polymer-modified bitumen	64	−18	58

results from bending-beam experiments of *pure* bitumen are presented, allowing one to identify parameters describing the low-temperature creep of bitumen. Then, upscaling of these properties for bitumen-filler composites is described, using the creep parameters for *pure* bitumen as input. Finally, the result of the employed upscaling scheme, providing estimates for the creep parameters for the bitumen-filler composite, is assessed by additional bending-beam experiments, providing insight into the mechanical contribution of filler on the composite behavior.

Materials and Methods

In order to cover a wide range of different bitumen-filler combinations, five types of bitumen, ranging from very soft to air-blown (very hard) bitumen (see Table 1, bitumen notation according to ÖNORM EN 12591 1999), and four types of filler were considered in the experimental program (see Table 2 and Fig. 2).

The fillers vary in the specific surface, mineralogy (acid or alkaline), grain shape, and grading curve (see Fig. 2). Following the multiscale concept mentioned in the Introduction, experiments for the identification of filler properties were conducted, providing: (1) the real mass density ρ_f (pycnometer) (ÖNORM EN 1097-6 2001); (2) the air voids f_a [Ridgen test (Ridgen 1954) (ÖNORM EN 1097-4 1999)]; and (3) the specific surface [Brunauer–Emmett–Teller (BET) method (Brunauer et al. 1938)].

For the determination of creep parameters of *pure* bitumen and mastic, bending-beam experiments were performed. The employed bending-beam rheometer (BBR) is a three-point bending-beam test, designed to characterize the low-temperature behavior of bituminous binders. Hereby, a beam-shaped specimen with the dimensions $125 \times 12.5 \times 6.25$ mm is placed horizontally on two bearings (spacing $\ell = 102$ mm) which are submerged into an ethyl

Table 2. Properties of Fillers Considered in the Experimental Program

Type of filler	Mineralogy	Real mass density ρ_f [kg/m^3]	Air voids[a] f_a^R [vol-%]	Surface [m^2/kg]
Hydrated lime	Lime	2,230	64.0	15,800
Limestone dust	Calcite, dolomite	2,710	30.5	2,050
Magyer	Quartz, dolomite, calcite, mica, feldspar	2,760	35.2	4,990
Schremser granite	Mica, quartz, feldspar	2,700	37.1	2,580

[a]Air void content obtained from Ridgen test (Ridgen 1954) (ÖNORM EN 1097-4 1999).

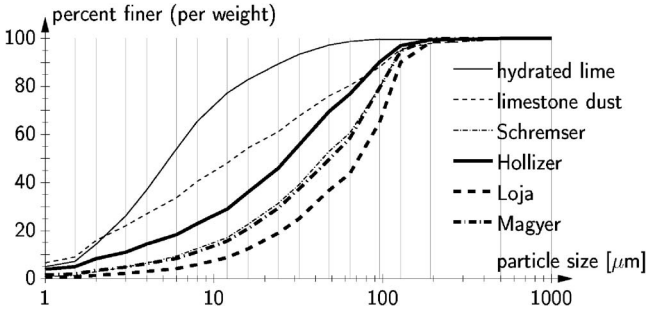

Fig. 2. Grading curve of fillers considered in the experimental program

alcohol bath, providing a constant prespecified temperature. In standard BBR testing, a load F of 980 mN is applied for four minutes at the midspan of the beam (see Fig. 3) (Cannon Instrument Company 1998).

Commonly, the creep stiffness S is computed from the monitored displacement history $u(t)$, using the linear-elastic beam theory, as

$$S(t) = \frac{F\ell^3}{4bh^3u(t)} \tag{1}$$

where b, h, and ℓ refer to the width, height, and the length of the beam, respectively. In addition to the creep stiffness, a so-called m value, referred to as the logarithmic creep rate is determined. The m value represents the slope of tangent to $\log S - \log t$ graph at $t = 60$ s (SHRP 1994). The extension of formulas derived from the beam theory based on the linear-elastic material response to viscoelastic material behavior, as done in Eq. (1), is only valid if both the strain and stress distribution over the cross section of the beam remain linear. This, on the other hand, implies that the evolution of the creep strain depends linearly on the applied stress. In order to validate the linearity of the underlying creep process, BBR tests characterized by three different load levels were performed. In addition to the standard load of 980 mN, a load of 490 and 1,960 mN were considered. Fig. 4 shows the measured displacement after 4 min, normalized by the applied load F, as a function of F. The obtained results clearly indicate the linearity of the underlying creep behavior, with u/F= constant and, hence, $u = \text{constant} \times F$. In the case of a linear-elastic material behavior, the stress at the bottom fiber of the midspan cross section and the respective deflection of this cross section are given by

$$\sigma = \frac{F\,\ell/4}{bh^2/6} \quad \text{and} \quad u = \frac{F\ell^3}{48EI} \tag{2}$$

Considering Eqs. (2) in $\varepsilon = \sigma/E$ gives the strain in the bottom fiber as a function of the measured displacement, reading

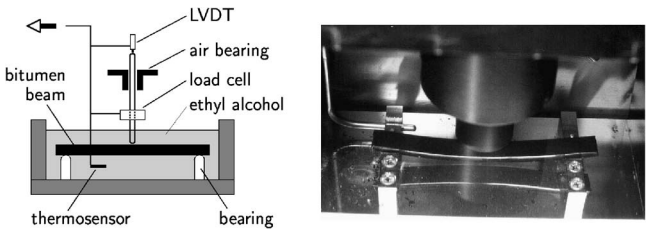

Fig. 3. Bending-beam rheometer: experimental setup

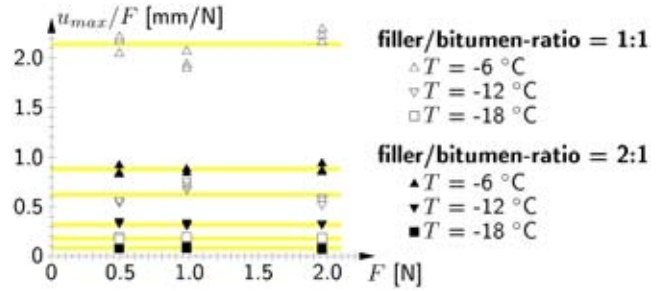

Fig. 4. Maximum deflection obtained from bending-beam rheometer experiments after 4 min of loading considering different load levels (B70/100, limestone-dust filler, filler/bitumen-ratio represents mass ratio)

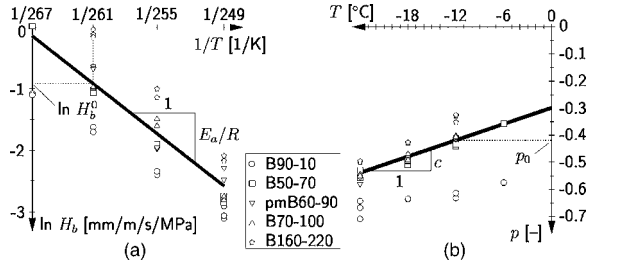

Fig. 6. H and p determined for different types of bitumen at different temperatures: (a) identification of Arrhenius law describing the temperature dependence of H_b and (b) linear relation between p and T

$\varepsilon = 6hu/\ell^2$. Finally, the elastic compliance $1/E$ [MPa^{-1}] is obtained in the form

$$\frac{1}{E} = \frac{\varepsilon}{\sigma} = \frac{4bh^3}{F\ell^3} u \text{ [MPa}^{-1}\text{]} \tag{3}$$

In case of linear creep, Eq. (3) can be applied to the displacement history measured during BBR tests, yielding the creep compliance J [MPa^{-1}] as a function of time, with $J(t) \propto u(t)$. In the remaining part of the paper, the creep compliance J [MPa^{-1}] and the creep-compliance rate dJ/dt [MPa^{-1} s^{-1}] will be used instead of the commonly employed parameter S and the m value.

Low-Temperature Creep of Bitumen

In order to avoid the interpretation of experimental results on the basis of the empirical parameters S and m (SHRP 1994), rheological models for pure bitumen were employed in order to identify creep characteristics from bending-beam experiments such as e.g., Burger's model, as reported in (Johansson and Isacsson 1998). The creep compliance of Burger's model for a testing time of four minutes is illustrated in Fig. 5(a). However, when extending the testing time of the BBR experiment to 1 h [as depicted in Fig. 5(b)], the continuous decrease of the compliance rate cannot be reproduced by Burger's model.

As a remedy, the identification of parameters with a clear physical background is proposed in this paper. For this purpose, the creep compliance rate dJ/dt, commonly plotted in the $\log dJ/dt - \log t$ diagram [see Fig. 5(c)], is approximated by a linear function, reading

$$dJ/dt \approx H(t/\tau)^p \tag{4}$$

where the constant time parameter τ is set equal to 1 s. Integration of Eq. (4) gives the creep compliance as $J(t) \approx J_0 + Ht^{p+1}/\tau^p/(p+1)$. In Eq. (4), H [MPa^{-1} s^{-1}] represents the creep compliance rate at $t=\tau$ and p [–] is the slope of the linear approximation function in the $\log dJ/dt - \log t$ diagram, with $p<0$. In the following, the parameters H and p are obtained from a least-squares minimization problem, aiming at best possible match between the experimental results and the approximation function $H(t/\tau)^p$ within the time interval $30<t<230$ s [see Fig. 5(c)].

Fig. 6 shows the values for H and p determined from BBR results of the bitumens considered in this study. The increase of p with increasing temperature is related to changes in the bitumen microstructure. This microstructure is characterized by the coexistence of parts in both the glassy and the viscous (rubberlike) state, resulting from the molecular cocktail in bitumen, comprising saturates, aromates, resins, and asphaltenes. Moreover, the large-size polar molecules (resins and asphaltenes) aggregate to stringlike structures. Whereas these structures seem to remain within the considered temperature range from −24 to 0°C, the glassy part in bitumen composed of resins, aromates, and saturates, decreases with increasing temperature and, hence, the creep capacity increases. This is reflected by the increase of p with increasing temperature. Based on the experimental results, $p(T)$ may be approximated by a linear function, reading [see Fig. 6(b)]

$$p(T) = p_0 + c(T - \bar{T}) \quad \text{(with } T \text{ in [°C] and } \bar{T} = -12\text{°C)} \tag{5}$$

where p_0 [–] and c [°C^{-1}]=constant parameters, which need to be specified for the different types of bitumen. In case of B70/100, $p_0 = -0.42$ and $c = 0.01$ °C^{-1} [see Fig. 6(b)]. Whereas the

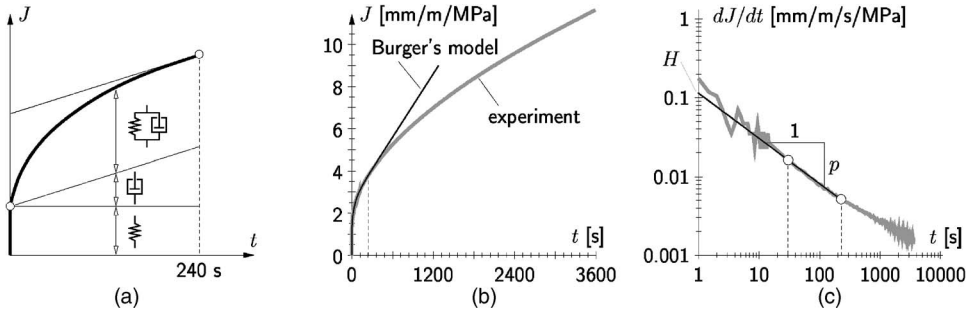

Fig. 5. Creep compliance of Burger's model: (a) different contributions to compliance (b) comparison with experimental data; and (c) experimental result for creep-compliance rate dJ/dt (B70/100, F=980 mN, T=−18°C)

change of the slope of the compliance rate is associated with changes in the microstructure of bitumen the increase of the compliance of pure bitumen, represented by the value of H_b, with increasing temperature is related to increased mobility of the molecules. This increase of mobility is accounted for by an Arrhenius-type law, reading

$$H_b = H_b^0 \exp\left[-\frac{E_a}{R}\left(\frac{1}{T} - \frac{1}{\bar{T}}\right)\right]$$

$$(\text{with } T \text{ in [K] and } \bar{T} = 273\text{–}12 \text{ K}), \qquad (6)$$

or, respectively

$$\ln H_b = \left(\ln H_b^0 + \frac{E_a}{R\bar{T}}\right) - \left(\frac{E_a}{R}\right)\frac{1}{T} \qquad (7)$$

[see Fig. 6(a)] where R=gas constant, with 8.31 J/Mol/K. According to Fig. 6(a), H_b^0 [MPa^{-1}] and the activation energy E_a [J/Mol] for B70/100 are obtained as H_b^0=0.0004 MPa^{-1} s^{-1} and E_a/R=9,000 K. In fact, the identified parameters p_0, c, H_0, and E_a, describing low-temperature creep of bitumen, depend on the molecular composition of the considered bitumen and should be related to the glassy-viscous (rubberlike) state. Within the multiscale model, this dependency is addressed at the *bitumen*-scale which is not the focus of this paper. In the following, Eqs. (5) and (6) with the parameters given for B70/100 will be used to describe low-temperature creep of the bitumen phase in the mastic.

Filler-Bitumen Interaction — Low-Temperature Creep of Mastic

For the homogenization of the low-temperature creep behavior of the bitumen-filler composite, continuum micromechanics is employed (see, e.g., Suquet 1997). Following the three-step procedure of continuum micromechanics, the following subsections deal with: (1) the representation; (2) the localization; and (3) the homogenization of the bitumen-filler composite.

Representation

The representation of a material is comprised of the definition of homogeneous constituents (material phases) as well as their assemblages. Whereas the employed multiscale model comprises five observation scales (Fig. 1), homogenization dealt with in this paper is performed on the *mastic*-scale only. The length of the representative volume element (RVE) of the *mastic*-scale must be both considerably larger than the filler dimensions and considerably smaller than the size of the RVE representing the next higher scale, the *mortar*-scale. Accordingly, the RVE of the *mastic*-scale has the size of approximately 1 mm and consists of inclusions (filler particles) embedded in the bitumen matrix (two-phase system, see Fig. 7). The volume fraction of the filler at the *mastic*-scale, f_f [−], is determined from the volume of bitumen and filler, V_b [m^3] and V_f [m^3], reading

$$f_f = \frac{V_f}{V_b + V_f} = \frac{m_f/\rho_f}{m_b/\rho_b + m_f/\rho_f} = \frac{(m_f/m_b)/\rho_f}{1/\rho_b + (m_f/m_b)/\rho_f} \qquad (8)$$

where the ratio between the filler mass m_f and the bitumen mass m_b, m_f/m_b-ratio, is specified in BBR experiments. In Eq. (8), ρ_f is the filler density, given in Table 2, and the density of bitumen ρ_b equals 1,030 kg/m^3.

In regard to the creep properties of the constituents at the *mastic*-scale, viscous deformations of the filler fraction are assumed to be zero. This assumption is reasonable since under typical loading situations, the filler exhibits only an elastic material response.

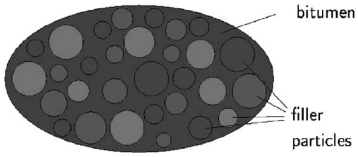

Fig. 7. Micromechanical model: representative volume element for bitumen-filler composite (matrix-inclusion morphology; matrix: bitumen; inclusions: filler particles)

Localization and Homogenization

The local strain tensor in the bitumen and filler phases at the *mastic*-scale, $\boldsymbol{\varepsilon}_b$ and $\boldsymbol{\varepsilon}_f$, are related to the homogeneous strain tensor $\mathbf{E}$ by the so-called localization tensor $\mathbb{A}$, reading

$$\boldsymbol{\varepsilon}_b(\mathbf{x}) = \mathbb{A}_b(\mathbf{x}):\mathbf{E} \quad \text{and} \quad \boldsymbol{\varepsilon}_f(\mathbf{x}) = \mathbb{A}_f(\mathbf{x}):\mathbf{E} \qquad (9)$$

The stiffness tensor $\mathbb{C}$ of the homogeneous material is obtained by the introduction of constitutive relations for the different phases, with $\mathbb{c}$ as the local phase stiffness tensor, reading

$$\boldsymbol{\Sigma} = \langle\boldsymbol{\sigma}\rangle_V = \langle\mathbb{c}:\boldsymbol{\varepsilon}\rangle_V = \langle\mathbb{c}:\mathbb{A}\rangle_V:\mathbf{E} \equiv \mathbb{C}:\mathbf{E} \qquad (10)$$

giving

$$\mathbb{C} = \langle\mathbb{c}:\mathbb{A}\rangle_V \qquad (11)$$

where $\langle\cdot\rangle_V = 1/V \int_V \cdot dV$=volume average; and $\boldsymbol{\Sigma}$ represents the homogeneous stress tensor. An estimate for the homogenized stiffness tensor follows from Eq. (11), reading

$$\mathbb{C}^{\text{est}} = f_b\mathbb{c}_b:\mathbb{A}_b^{\text{est}} + f_f\mathbb{c}_f:\mathbb{A}_b^{\text{est}} \qquad (12)$$

where f_r, $\mathbb{c}_r$, and $\mathbb{A}_r^{\text{est}}$ denote the volume fraction, the stiffness, and the estimate for the localization tensor of the rth phase. In case of an inclusion-matrix morphology as depicted in Fig. 7, the estimate for the yet unknown localization tensor is provided by the Mori–Tanaka (MT) scheme (Mori and Tanaka 1973) as

$$\mathbb{A}_f^{\text{est}} = [\mathbb{I} + \mathbb{S}_f:(\mathbb{c}_b:\mathbb{c}_f - \mathbb{I})]^{-1}:\langle[\mathbb{I} + \mathbb{S}_f:(\mathbb{c}_b:\mathbb{c}_f - \mathbb{I})]^{-1}\rangle_V^{-1} \qquad (13)$$

where $\mathbb{S}_f$=Eshelby tensor of the filler phase. The localization tensor for the bitumen matrix is obtained from $\langle\mathbb{A}\rangle_V = \mathbb{I}$.

Because of the absence of air voids at the *mastic*-scale (see Fig. 7), viscous deformations may only result from deviatoric creep. Accordingly, the homogenized shear modulus is obtained from Eq. (12), considering $\mathbb{A}_b^{\text{est}}$ and $\mathbb{A}_f^{\text{est}}$, with $\mathbb{S}_f$ specialized for spherical inclusions, as

$$\mu^{\text{est}} = \mu_b + \frac{f_f(\mu_f - \mu_b)}{1 + (1 - f_f)\beta(\mu_f/\mu_b - 1)} = \mu_b + \frac{f_f(1 - \mu_b/\mu_f)}{1/\mu_f + (1 - f_f)\beta(1/\mu_b - 1/\mu_f)} \qquad (14)$$

where μ_b and μ_f refer to the shear modulus of bitumen and filler, respectively. In Eq. (14), β represents the respective entry of the fourth-order Eshelby tensor, reading for spherical inclusions

$$\beta = \frac{6(k_b + 2\mu_b)}{5(3k_b + 4\mu_b)} = \frac{6(1 + 2\mu_b/k_b)}{5(3 + 4\mu_b/k_b)} \tag{15}$$

where k_b represents the bulk modulus of bitumen. Assuming in the following the bitumen phase to be incompressible ($k_b \to \infty$) and considering the filler particles as rigid inclusions ($\mu_f \to \infty$), Eq. (12) becomes

$$\mu^{\text{est}} = \mu_b + \frac{f_f}{(1 - f_f)2/5/\mu_b} = \mu_b\left(1 + \frac{5}{2}\frac{f_f}{1 - f_f}\right) \tag{16}$$

Based on the estimate for the shear modulus of the homogenized material given in Eq. (16), the creep parameter H, representing the initial compliance rate of the homogenized material, is estimated from

$$H^{\text{est}} = H_b(H_b^0, T) \times \left(1 + \frac{5}{2}\frac{f_f}{1 - f_f}\right)^{-1} \tag{17}$$

where H_b represents the creep parameter H for the bitumen matrix, available from Eq. (6). A similar expression for the viscosity, which is proportional to $1/H$, was obtained by Chow (1993) for concentrated dispersions starting from Stokesian dynamics.

Comparison with Experimental Data

Eq. (17) is used for the estimation of the creep parameter H for different bitumen-filler composites made of B70/100 and the fillers listed in Table 2. The obtained results are shown in Fig. 8.

The prediction of the creep parameter H by Eq. (17) results in a significant overestimation of the respective experimental data. For all types of filler, in Fig. 8, this is indicated for the results corresponding to $T = -6$°C. However, a similar situation is observed for the other experimental results obtained from different testing temperatures. For bending-beam experiments characterized by a creep parameter H exceeding 0.4 mm/m/s/MPa (see testing temperature of 0°C), the rather high compliance of the tested bitumen-filler composite resulted in deflections of the bending beam reaching 4 mm. The geometrical effects in consequence of a deflection/span-ratio of $4/102 \approx 1/25$, however, are not captured by Eqs. (2) and (3), which were derived for the geometrically linear situation.

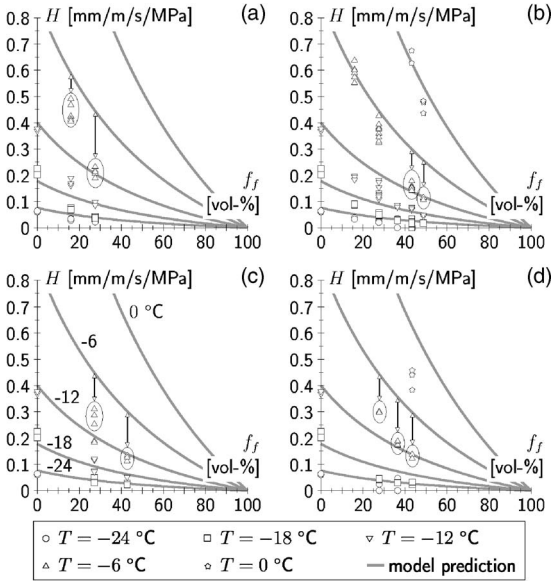

Fig. 8. Validation of micromechanical model for mastic consisting of B70/100 and (a) hydrated-lime, (b) limestone-dust, (c) Magyer, and (d) Schremser filler (used parameters: $H_b^0 = 0.4$ mm/m/s/MPa, $E_a/R = 9{,}000$ K)

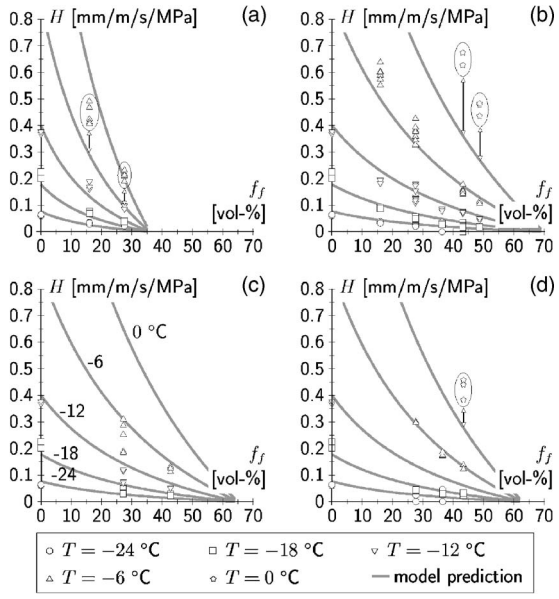

Fig. 9. Validation of micromechanical model for mastic consisting of B70/100 and (a) hydrated-lime, (b) limestone-dust, (c) Magyer, and (d) Schremser filler employing the *effective* volume concept (used parameters: $H_b^0 = 0.4$ mm/m/s/MPa, $E_a/R = 9{,}000$ K)

As a remedy for the observed overestimation of H by Eq. (17), the consideration of the *effective* volume content of the filler is proposed (see, e.g., Ewers and Heukelom 1964; Gillespie 1982). The *effective* volume of the filler comprises the volume of the filler particles f_f and the volume of the air voids f_a^R in case of maximum filler compaction. For the determination of the latter, the Ridgen experiment (Ridgen 1954) (ÖNORM EN 1097-4 1999) is employed (see Table 2). The packing volume is obtained from f_a^R as $1/(1 - f_a^R)$. Replacing f_f in Eq. (17) by the *effective* filler content $f_f/(1 - f_a^R)$, with $f_f/(1 - f_a^R) > f_f$, yields

$$H^{\text{est}} = H_b(H_b^0, T) \times \left(1 + \frac{5}{2}\frac{f_f/(1 - f_a^R)}{1 - f_f/(1 - f_a^R)}\right)^{-1} \tag{18}$$

The creep parameter H^{est} obtained from Eq. (18) agrees very well with the experimentally-obtained values for H (see Fig. 9). The deviations observed in Figs. 9(b and d) are explained by the large compliance of the mastic at a testing temperature of 0°C. The underestimation of H in Fig. 9(a) for $T = -6$°C, on the other hand is explained by the consistency and high viscosity of mastic containing hydrated-lime filler (especially for filler volume fractions exceeding 25%), resulting from the large specific surface of hydrated lime (see Table 2).

In addition to the creep parameter H, the influence of the amount of filler on the slope p of the linear approximation function in the $\log dJ/dt - \log t$ diagram is investigated. Fig. 10 shows the experimentally obtained values for p for mastic consisting of B70/100 and the fillers listed in Table 2 as well as the result of Eq. (5), assuming a linear relation between p and T, with $p_0 = -0.42$ and $c = 0.01\,°\text{C}^{-1}$. Although a slight decrease of p is observed for increasing filler content, the value of p seems to be determined by the behavior of the used bitumen and the temperature. All values for p are found in the range from -0.60 to -0.25,

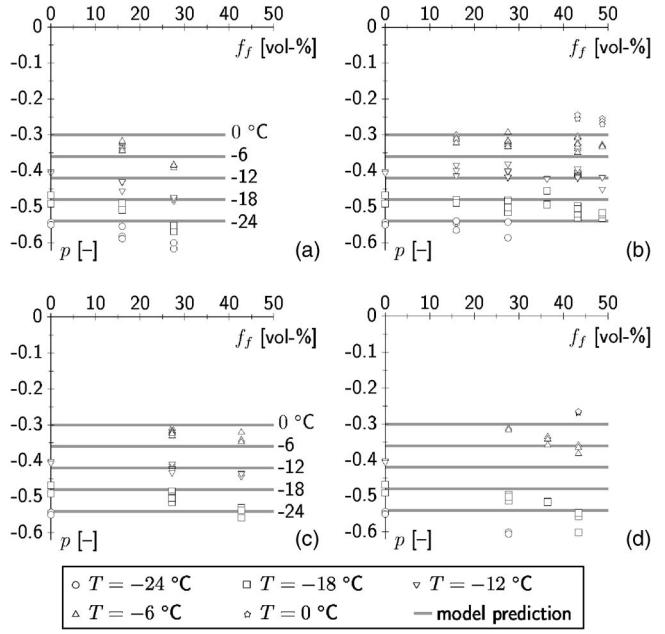

Fig. 10. Predicted and measured creep parameter p for mastic consisting of B70/100 and (a) hydrated-line, (b) limestone-dust, (c) Magyer, and (d) Schremser filler (used parameters: p_0=−0.42, c=0.01°C^{-1})

independent of the type of filler. Finally the estimated values for the creep parameters H and p by Eqs. (18) and (5) are compared to the experimental results for all considered types of bitumen and fillers (see Tables 1 and 2). For this purpose, the parameters of *pure* bitumen H_b^0, E_a/R, and p_0, and c, already identified for B70/100, are determined for the remaining types of bitumen (see Table 3).

Remarkably, since E_a/R and c are assumed to be constant for all types of bitumen, low-temperature creep is fully described by only two parameters, namely, H_b^0 and p_0 (see Table 3). The obtained results are plotted in Fig. 11, showing excellent agreement between the experimental data and the prediction by the micromechanical model. As already observed in Fig. 9, geometrical effects in the case of large deflections of the bending beam cause an increase of the deflection and, hence, a shift of the value for the parameter H [see Fig. 11(a)].

Conclusions

In this paper, the effect of filler on low-temperature creep of asphalt mastic was investigated. After identification of two creep parameters derived from the creep compliance rate obtained from

Table 3. Parameters Describing Low-Temperature Creep of the (*pure*) Bitumens Considered in the Experimental Program

Type of bitumen	H_b^0 [mm/m/s/MPa]	E_a/R [K]	p_0 [–]	c [°C^{-1}]
B90/10	0.21	9,000	−0.60	0.01
B50/70	0.34	9,000	−0.44	0.01
B70/100	0.40	9,000	−0.42	0.01
pmB60/90	0.51	9,000	−0.42	0.01
B160/220	0.71	9,000	−0.36	0.01

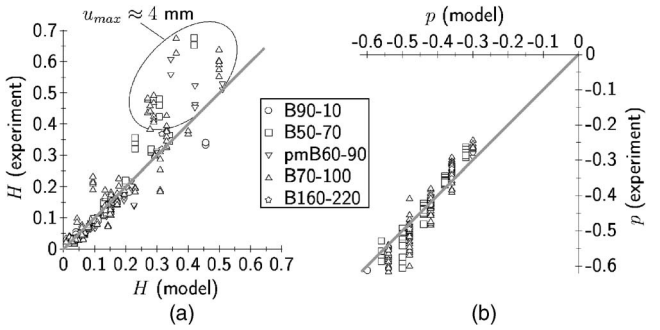

Fig. 11. Comparison between experimental results for creep parameters (a) H [mm/m/s/MPa] and (b) p [–] and the prediction by the micromechanical model via Eqs. (18) and (5) (all types of bitumens and all types of fillers included, 306 bending-beam rheometer experiments)

bending-beam experiments for *pure* bitumen, a multiscale model employing the MT scheme for homogenization at the so-called *mastic*-scale was used for the prediction of the respective creep parameters for the bitumen-filler composite. Based on the characteristics of the underlying MT scheme and the good agreement between the so-obtained creep parameters and results from bending-beam experiments of asphalt mastic, the following conclusions can be drawn.

- According to the specifications of the underlying MT scheme, the filler influences low-temperature creep in form of rigid inclusions randomly distributed within the viscous bitumen matrix.
- Moreover, consideration of filler as idealized spherical inclusions within the MT scheme suggests that only the volume fraction of the filler has an effect on the creep properties of the bitumen-filler composite. The shape of the filler particles, on the other hand, does not significantly influence low-temperature creep.
- Whereas the filler significantly influenced the initial value of the creep compliance dJ/dt (denoted as H), it had almost no effect on the reduction of dJ/dt with time, described by the parameter p. The latter was mainly affected by the type of the bitumen used, rather than of the type and the amount of filler.

Based on the given conclusions and considering that several types of bitumen and filler were included in the present study, low-temperature creep seems to be independent of filler shape and mineralogy. The extension of these findings to medium-/high-temperature creep of asphalt mixes, however, is not straightforward. In contrast to low-temperature creep, the filler particles start to rotate and aggregate at higher temperatures, increasing the effect of filler on the viscous behavior of the bitumen-filler composite. The consideration of these effects within the developed multiscale model is a topic of ongoing research.

Acknowledgments

The writers thank Babara Gagliano, Andreas Jäger, Karl Kappl, and Michael Wistuba from the Christian Doppler Laboratory for "Performance-based Optimization of Flexible Pavements" for fruitful discussions and helpful comments. The writers are indebted to Martin Hopfgartner, Thomas Riedmayer, Johann Schuch, and Roman Slany for the conduction of the bending-beam experiments. Financial support by the Christian

Doppler Forschungsgesellschaft (Vienna, Austria) is gratefully acknowledged.

Notation

The following symbols are used in this paper:

$\mathbb{A}$ = localization tensor;
$\mathbb{A}_b$ = localization tensor of bitumen;
$\mathbb{A}_f$ = localization tensor of filler;
b = width of bending-beam rheometer bitumen/mastic beam;
$\mathbb{C}$ = stiffness tensor of homogeneous material;
c = parameter describing dependence of p on T;
$\mathbb{c}$ = material tensor of single phase;
$\mathbb{c}_b$ = material tensor of bitumen;
$\mathbb{c}_f$ = material tensor of filler;
$\mathbf{E}$ = homogeneous strain tensor;
E = Young's modulus;
E_a = activation energy;
F = load applied in bending-beam rheometer experiments;
f_a^R = volume fraction of air obtained from Ridgen test;
f_b = volume fraction of bitumen;
f_f = volume fraction of filler;
H = initial creep compliance rate;
H_b = initial creep compliance rate of pure bitumen;
H_b^0 = value of H_b at $T=\bar{T}$;
h = height of bending-beam rheometer bitumen/mastic beam;
$\mathbb{I}$ = fourth-order unity tensor;
I = moment of inertia;
J = creep compliance;
J_0 = elastic compliance;
k_b = bulk modulus of bitumen;
ℓ = length of bending-beam rheometer bitumen/mastic beam;
m_b = mass of bitumen;
m_f = mass of filler;
p = slope of creep compliance rate in $\log dJ/dt - \log t$ diagram;
p_0 = value of p at $T=\bar{T}$;
R = gas constant, with $R=8.31$ J/Mol/K;
S = secant stiffness monitored during bending-beam rheometer experiments;
$\mathbb{S}_f$ = fourth-order Eshelby tensor for filler particles;
T = temperature;
$\bar{T}$ = reference temperature;
t = time;
u = midspan deflection of bending-beam rheometer beam;
$u_{\max}$ = maximum midspan deflection of bending-beam rheometer beam after 240 s;
V = volume of representative volume element;
V_b = volume of bitumen;
V_f = volume of filler;
V_p = packing volume;
$\mathbf{x}$ = spatial coordinate vector;
β = quantity representing the Eshelby tensor in case of spherical inclusions;
ε = strain;
$\boldsymbol{\varepsilon}$ = local strain tensor;
$\boldsymbol{\varepsilon}_b$ = local strain tensor in bitumen;
$\boldsymbol{\varepsilon}_f$ = local strain tensor in filler;
μ = shear modulus;
μ_b = shear modulus of bitumen;
μ_f = shear modulus of filler;
ρ_b = density of bitumen;
ρ_f = density of filler;
$\boldsymbol{\Sigma}$ = homogeneous stress tensor;
$\boldsymbol{\sigma}$ = local stress tensor;
σ = stress; and
τ = constant time parameter, with $\tau=1$ s.

References

Brunauer, S., Emmett, P., and Teller, E. (1938). "Adsorption of gases in multimolecular layers." *J. Am. Chem. Soc.*, 60, 309–319.

Cannon Instrument Company. (1998). *Cannon Bending-Beam Rheometer with Software for Windows 95 and NT—Instruction & Operation Manual for BBR and TE-BBR models. Version 1.1a*, Cannon Instrument Company.

Chow, T. (1993). "Viscosities of concentrated dispersions," *Phys. Rev. E*, 48(3), 1977–1983.

Ewers, J., and Heukelom, W. (1964). "Die Erhöhung der Viskosität von Bitumen durch die Zugabe von Füller [The increase of bitumen viscosity by the allowance of filler]." *Straße und Autobahn*, (2), 31–39, in German.

Gillespie, T. (1982). "The effect of aggregation and particle size distribution on the viscosity of newtonian suspensions." *J. Colloid Interface Sci.*, 94(1), 166–173.

Jäger, A. (2004). "Microstructural identification of bitumen by means of atomic force microscopy (AFM), modulated differential scanning calorimetry (MDSC), and reflected light microscopy (RLM)." MS thesis, Vienna Univ. of Technology, Vienna, Austria.

Johansson, L., and Isacsson, U. (1998). "Effect of filler on low-temperature physical hardening of bitumen." *Constr. Build. Mater.*, 12, 463–470.

Mori, T., and Tanaka, K. (1973). "Average stress in matrix and average elastic energy of materials with misfitting inclusions." *Acta Metall.*, 2l, 571–574.

ÖNORM EN 1097–4. (1999). *Tests for mechanical and physical properties of aggregates—Part 4: Determination of the voids of dry compacted filler*, Österreichisches Normungsinstitut.

ÖNORM EN 1097–6. (2001). *Tests for mechanical and physical properties of aggregates—Part 6: Determination of particle density and water absorption*, Österreichisches Normungsinstitut.

ÖNORM EN 12591. (1999). *Bitumen and bituminous binders—Specifications for paving grade bitumens*, Österreichisches Normungsinstitut.

Ridgen, P. (1954). "The rheology of nonaqueous suspensions." *Road Research Technical Papers*, *28*.

Shell-Bitumen-U.K. (1990). *The Shell bitumen handbook*, Vol. 1. Shell Bitumen U.K., Chertsey.

Strategic Highway Research Program (SHRP). (1994). "Binder characterization and evaluation. Volume 4: Test methods." *SHRP-A-370*, National Research Council, Washington, D.C.

Suquet, P., ed. (1997). *Continuum micromechanics*, Springer, Wien.